

Received February 25, 2019, accepted March 28, 2019, date of publication April 1, 2019, date of current version April 16, 2019.

Digital Object Identifier 10.1109/ACCESS.2019.2908724

A Deep Learning Approach for Breast Invasive Ductal Carcinoma Detection and Lymphoma Multi-Classification in Histological Images

NADIA BRANCATI¹, GIUSEPPE DE PIETRO¹, (Member, IEEE),
MARIA FRUCCI¹, AND DANIEL RICCIO^{1,2}, (Member, IEEE)

¹Institute for High Performance Computing and Networking National Research Council of Italy (ICAR-CNR), 80131 Naples, Italy

²Department of Electrical Engineering and Information Technology, University of Naples Federico II, 80138 Naples, Italy

Corresponding author: Nadia Brancati (nadia.brancati@cnr.it)

ABSTRACT Accurately identifying and categorizing cancer structures/sub-types in histological images is an important clinical task involving a considerable workload and a specific subspecialty of pathologists. Digitizing pathology is a current trend that provides large amounts of visual data allowing a faster and more precise diagnosis through the development of automatic image analysis techniques. Recent studies have shown promising results for the automatic analysis of cancer tissue by using deep learning strategies that automatically extract and organize the discriminative information from the data. This paper explores deep learning methods for the automatic analysis of Hematoxylin and Eosin stained histological images of breast cancer and lymphoma. In particular, a deep learning approach is proposed for two different use cases: the detection of invasive ductal carcinoma in breast histological images and the classification of lymphoma sub-types. Both use cases have been addressed by adopting a residual convolutional neural network that is part of a convolutional autoencoder network (i.e., FusionNet). The performances have been evaluated on the public datasets of digital histological images and have been compared with those obtained by using different deep neural networks (UNet and ResNet). Additionally, comparisons with the state of the art have been considered, in accordance with different deep learning approaches. The experimental results show an improvement of 5.06% in F-measure score for the detection task and an improvement of 1.09% in the accuracy measure for the classification task.

INDEX TERMS Histological images, deep learning, multi-classification, detection.

I. INTRODUCTION

The digitalization of histological specimens by using modern whole-slide digital scanners brings not only the advantage of an easy storage, visualization, and analysis of the images, but also affords the possibility of applying automatic image analysis techniques to digital histological slides to provide accurate quantifications (e.g., tumor extent and nuclei counts) and classifications of tumor sub-types with the aim both of reducing inter- and intra-reader variability among pathologists and of accelerating the diagnosis process. Any automatic analysis of digital histological images is a very challenging task, since both the spatial arrangement of the structures, e.g. nuclei and stroma, and the color distribution can be very different, also for images belonging to the same tumor class.

The associate editor coordinating the review of this manuscript and approving it for publication was Yudong Zhang.

Deep learning (DL) approaches are particularly suitable to address these problems and to perform tasks, such as the detection of specific areas of the disease or the discrimination between the tumor classes of interest. Indeed, especially when a large number of samples are available for training, a DL system learns representative features automatically and directly from the digital images of tumor tissue, with the goal of obtaining a maximum separability between the classes of structures or tumor sub-types.

In such a context, this paper presents a DL approach addressing two different use cases: i) the detection of invasive ductal carcinoma (IDC) of breast cancer, and ii) the lymphoma multi-classification in chronic lymphocytic leukemia (CLL), follicular lymphoma (FL), and mantle cell lymphoma (MCL).

IDC is the most common form of invasive breast cancer and its precise detection on whole-slide images (WSI) is crucial

to the diagnosis and sub-sequent estimation of grading the tumor aggressiveness of breast cancer. Manual IDC detection is tedious and time-consuming for pathologists and could be influenced by significant inter- and intra-pathologist variability in the diagnosis and interpretation of specimens. The diagnosis of lymphoma is a problematic and difficult process for pathologists. Lymphoma is a type of cancer affecting the lymphatic system and it is classified in different sub-types. In particular, three of these sub-types, CLL, FL and MCL account for 70% of lymphoma cases. The most important diagnostic criterium for lymphoma are the morphological features of the tumor which can be interpreted by an experienced hematopathologist, in such a way as to make a further differentiation between malignancy types to guide treatment decisions.

Both detection and classification tasks increase the demand for a reduction of workloads and of inter- and intra-observer variability, and also imply sub-specialty requirements in pathology. As a result, there is a great interest in DL networks which have the potential to reduce these workloads and augment the diagnostic capabilities of pathologists. The choice of a DL network and the training strategy to apply for a given task, depend on the type of pathological analysis to be performed.

In this paper, both use cases are addressed by adopting the residual convolutional autoencoder FusionNet, in relation to two different scenarios:

- the convolutional autoencoder FusionNet is trained under a sparsity constraint in an unsupervised manner; and
- a residual convolutional neural network that is the encoding part of FusionNet is trained in a supervised manner.

In both scenarios, the features learned at the end of the encoding stage are used for the classification, by means of a softmax classifier. Indeed, also the IDC detection is addressed as a classification task, by splitting the WSI into patches and classifying each patch as IDC or non-IDC.

The performances of each scenario have been evaluated on public datasets [2], containing histological images acquired by using Hematoxylin and Eosin (H&E) staining technique and in relation to selected pathological use cases. We also investigated the performances of different DL networks (ResNet and UNet) for both use cases. Moreover, comparisons with different approaches in literature, working on the same datasets, have been taken into account. The performance evaluation of these methods has been given in terms of F-measure score and Balanced Accuracy (BAC) for the IDC detection and in terms of Accuracy for the lymphoma multi-classification. On observing the classification performance using overall validation and test accuracies, our second scenario has produced favorable results for both use cases. Moreover, our results outperform the state of the art. Our approach achieved the best quantitative results both for IDC detection (F-measure and BAC equal to 81.54% and 87.76%,

respectively) and for lymphoma multi-classification (Accuracy equal to 97.67%).

The rest of the paper is organized as follows: previous related works are presented in Section II; a description of the approach is presented in Section III; the experimental setup, comparative strategies and results for the two different use cases are discussed in Section IV; and finally, in Section V certain conclusions are drawn.

II. RELATED WORK

A large number of papers have been published concerning the detection and classification of histological images. Some papers propose methods that use various image processing and machine learning techniques (e.g. SVM and decision trees) exploiting low-level hand-crafted features, such as color, texture, or morphology [6], [18], [22], [25], [29], [30].

Most methods in literature for the analysis of histological images are based on DL networks (e.g., AlexNet, ResNet and UNet [11], [15], [21]), that automatically learn features that optimally represent the data for the problem at hand. In some cases DL networks are integrated with well-known classifiers (e.g., SVM, Random Forest and Adaboost), and the methods adopt appropriate training strategies (e.g., defined patches, pre-processing, parameter setting and selected loss function). Additionally, for a specific task, the performance of the different approaches depends on the adopted network and the developed training strategy. It is no coincidence that many teams in international competitions have adopted the same network architecture on the same dataset with different training strategies for a specific task, obtaining widely different results [3], [17], [24].

Most of these methods are based on the use of Convolutional Neural Networks (CNN) for the detection and classification tasks. In the context of the detection task, the method in [26] won the first place at the ISBI2016 Metastasis Detection Challenge [17], by adopting a CNN with 27 layers, while the method in [8] outperformed in terms of accuracy the other methods at the ICPR2014 MITOS-ATYPIA Challenge [1] by using deep cascaded CNN. For the detection of IDC, the method in [9] yielded the best quantitative results in comparison with approaches using hand-crafted image features on the dataset available for download at [2]. For the classification task, a CNN based on AlexNet was adopted in [23] in order to discriminate between benign and malignant breast cancer tumors. This approach outperformed the previously reported results obtained by other machine learning models trained with hand-crafted textural descriptors on the BreakHis dataset [22]. The authors in [4] proposed a comparison between two approaches (hand-crafted and CNN based) for the classification of breast cancer histological images, showing that their CNN architecture outperforms the state of the art on BreakHis dataset. Other interesting experimental results were obtained for the same dataset by the method proposed in [5] by classifying breast cancer histological images independently of the image magnification factor. Three different configurations of ResNet were used by

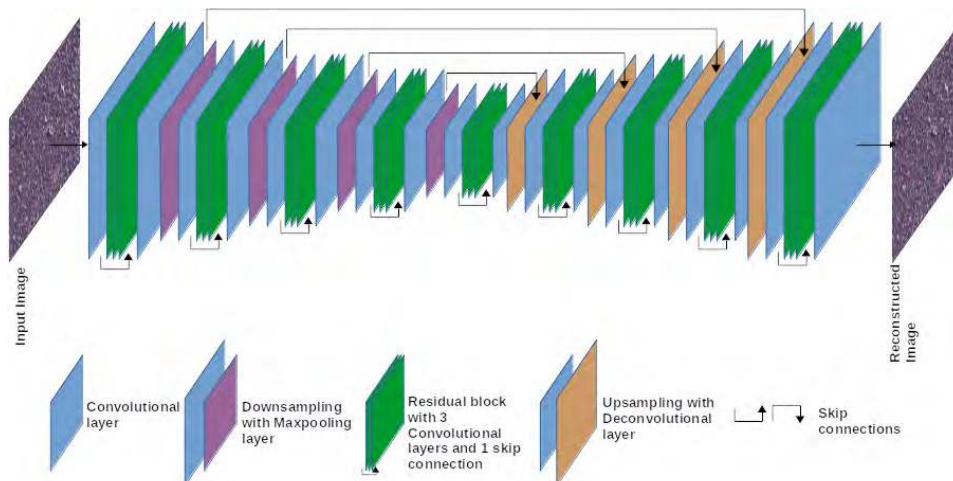


FIGURE 1. FusionNet architecture.

the authors in [7] for the multi-classification of breast cancer obtaining a remarkable performance on the images provided for the ICIAR2018 BACH Challenge [3]. Finally, in [13] AlexNet, using the same training strategy, was adopted both for IDC detection and lymphoma multi-classification on the datasets available for download at [2], outperforming the method proposed in [9], in relation to IDC detection.

Differently from the methods based on the CNN trained end-to-end technique for classification, other approaches have been based on unsupervised networks, mainly autoencoders (AE), that do not required labeled samples to detect the inner structure to be used for the subsequent detection and classification tasks. Indeed, AEs are commonly used for the pre-training of different deep neural networks or classifiers. An AE is optimized to learn the principal components of the data distribution. However, when a non-linear activation function is used, AE learns over complete unsupervised representations by reconstructing the original input, operating under several constraints (sparsity or hierarchicality) [19]. The authors in [10] employed sparse AEs to learn an unsupervised representation that feeds a softmax classifier over this representation identifying the image regions that are most relevant for the basal cell carcinoma cancer detection. In [12], a Convolutional Sparse AE for simultaneous nucleus detection and feature extraction in histological tissue images was proposed. The foreground image was reconstructed by certain vectors in feature maps that represent salient objects. Additionally, a Stacked Sparse AE framework was presented in [28] for automated nucleus detection on breast cancer histological images.

III. METHODOLOGY

The proposed approach is designed for IDC detection of and lymphoma multi-classification in H&E histological images. Differently from the segmentation process, the detection task does not involve the delineation of accurate boundaries for

the regions of interest, but only the identification of the areas including such regions. For this reason, the detection of IDC can be addressed as a classification problem: the WSI is divided into patches and the final detection is obtained by marking patches with an IDC or a non-IDC label.

The classification for both tasks is based on the use of a convolutional autoencoder (CAE), namely FusionNet [20]. Similarly to all CAE networks, the architecture of FusionNet has a configuration which is completely symmetrical, but it is also a residual network, due to the presence of skip connections (see Fig. 1).

FusionNet introduces long skip connections between the feature maps in the encoder and those located at the same level in the decoder; moreover, short skip connections are present in each residual block of the network. With such a configuration, the information flows within and across different levels of the network.

We propose two different scenarios for the classification:

- 1) Classification by reconstruction - the CAE is trained under a sparsity constraint in an unsupervised manner;
- 2) Supervised Classification - only the encoding part of the CAE is trained and this in a supervised manner.

In both cases, a softmax classifier takes the extracted features as the input. The output of the softmax classifier produces a value between 0 and 1 that can be interpreted as the probability of the input belonging to a given class. The classifier is trained minimizing the Cross Entropy Loss (CE), used to measure the divergence between the effective class c and the predictive class \hat{c} of n samples:

$$CE(c, \hat{c}) = - \sum_{i=1}^n c_i \cdot \log(\hat{c}_i) \quad (1)$$

In the first scenario, the network is trained in an unsupervised manner extracting features useful for the reconstruction of the input image. The obtained representation of the encoder

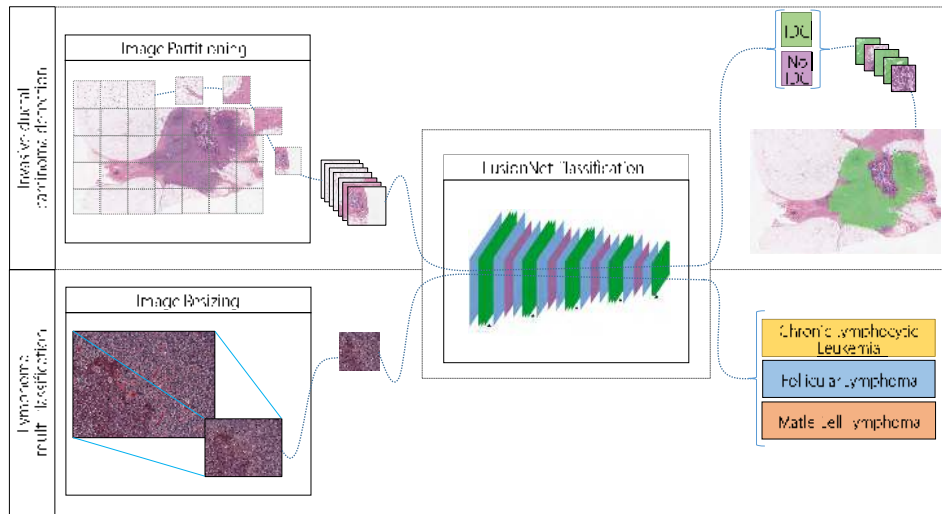


FIGURE 2. A graphical representation of SEF.

has a lower dimensionality than the input data. The set of weights associated with the representation can be interpreted as the set of feature maps learned by the CAE to be used for the classification. The Mean Squared Error Loss (MSE) is used to measure the error between the input image x and the reconstructed image \hat{x} :

$$MSE(x, \hat{x}) = \frac{\sum_{i=1}^n (x_i - \hat{x})^2}{n} \quad (2)$$

Backpropagation is implemented by using the Stochastic Gradient Descent (SGD) algorithm [16], with a controlled learning rate. In general, to improve the performance of an AE and to prevent overfitting, the addition of a sparsity constraint during the training is suitable [19], [28]. The sparsity constraint is imposed on the hidden units, enabling the AE to discover interesting structures in the data. We have imposed the sparsity constraint through the introduction of Kullback-Leibler divergence (KL), that measures the degree of difference between two distributions with means ρ and $\hat{\rho}_j$. In detail, ρ refers to the target activation function of the hidden units and $\hat{\rho}_j$ refers to the average activation function of the hidden unit j . The activation function used for the hidden units is the sigmoid function.

After the training, a maxpooling layer is applied to the extracted features and the output is passed to a fully connected layer that performs the classification by means of a softmax activation function. In this case, backpropagation is implemented by using the Adaptive Moment Estimation (Adam) algorithm [14], an extension of the SGD. The algorithm computes adaptive learning rates for each network parameter from estimates of first and second moments of the gradient.

In the second scenario, only the encoding part of the CAE is trained in a supervised manner, i.e. the input to the network is represented by the image and the corresponding class. The network is trained end-to-end to learn filters and to combine features with the aim of feeding a fully connected

layer. Also in this scenario, the Adam algorithm is used for backpropagation and a softmax activation function is used for the classification.

IV. USE CASES

The proposed approach is based on FusionNet. In particular, in the ‘‘Supervised Classification’’ scenario only the encoding part of FusionNet is trained, and therefore we refer to this approach as Supervised Encoder FusionNet (SEF). In Fig. 2, a graphical representation of SEF is shown. Moreover, both UNet and ResNet have been considered for comparison in the experiments. In the ‘‘Supervised Classification’’ scenario, we will refer to use of UNet as Supervised Encoder UNet (SEU), while no distinction will be needed for ResNet as it is not considered in the ‘‘Classification by reconstruction’’ scenario.

The performances have been evaluated on two datasets available for download at [2]. In the following section, we will refer to the datasets for IDC detection and for lymphoma multi-classification as D-IDC and D-Lymph, respectively. Regarding the implementation details, the framework has been implemented in Pytorch on a workstation equipped with 2 Xeon 10-Core E5-2630v4 2,2Ghz 25MB and 4 NVIDIA GEFORCE GTX 1080Ti 11GB PCI-EX.

In the following section, for each use case, details about the adopted dataset, the training strategy, and the experimental results compared with other approaches will be given.

A. INVASIVE DUCTAL CARCINOMA DETECTION

The experiments have been performed on the D-IDC dataset, which includes 162 WSI acquireFFTD at 40 \times , each partitioned into a set of patches with a size equal to 50 \times 50 pixels. The number of patches representing IDC and non-IDC is 46, 633 and 124, 011, respectively. An example of invasive ductal carcinoma is shown in Fig. 3.

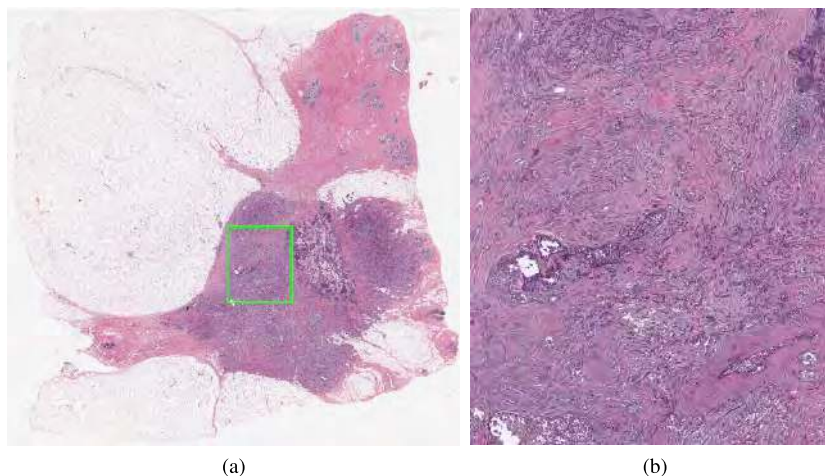


FIGURE 3. Invasive ductal carcinoma: (a) whole slide image; (b) a magnification of the highlighted box in (a).

TABLE 1. The training parameters for the IDC detection.

Scenario	N° Epochs	Mini-batch	Back. alg.	Init. Lear.rate	Lear.rate update
Classification by reconstruction	20	64	SGD	0.001	0.0001 after 15 th epoch
Supervised Classification	15	64	ADAM	0.0001	update by ADAM

TABLE 2. Results of the different approaches for the IDC detection. The best performance is highlighted in bold.

Scenario	Network	Acc.	F-meas.	Prec.	Sens.	Spec.	BAC
Classification by reconstruction	FusionNet	84.71	71.70	73.07	70.38	90.15	80.26
	UNet	84.65	68.30	79.14	60.07	93.99	77.03
Supervised Classification	SEF	89.57	81.54	79.45	83.75	91.77	87.76
	SEU	85.87	71.90	79.44	65.67	93.54	79.60
	ResNet-34	87.24	77.14	76.08	77.22	90.66	84.44

As shown in Fig. 1, the FusionNet encoder is composed of a set of blocks including downsampling layers. Whenever downsampling is performed, the input size is halved. This implies that the input image should have a size allowing for a scaling of factor 2 for each downsampling and guaranteeing that the input size of the bridge layer is not too small. In order to allow a scaling of factor 2, the input of the network is represented by the central square region of a size of 48×48 pixels, extracted from each patch. Since the encoder is constituted by 4 downsampling layers, the input size of the bridge layer is equal to 3×3 .

Since a large number of images are available, no augmentation operation has been performed. In order to allow for a comparison with the state of the art, the same training and testing sets as [9], [13] have been used. In particular, the training set consists of about 70% of the whole dataset. The final detection on each WSI will be given in terms of IDC or non-IDC patches.

The values of the parameters adopted for the training are given in Table 1. Both scenarios produce 512 feature maps,

subsequently used for the classification step. In the ‘‘Classification by reconstruction’’ scenario, a max pooling layer with a kernel size equal to 2×2 and a stride equal to 2 is applied at the end of the encoding stage, while in the second scenario the max pooling layer is substituted by a fully connected layer.

1) EXPERIMENTAL RESULTS AND DISCUSSION

We have compared the performance of the different approaches in terms of standard metrics, namely Accuracy, F-Measure, Precision, Sensitivity and Specificity. We evaluated the performance also in terms of the Balanced Accuracy (BAC) measure, calculated as the average between the Specificity and Sensitivity. The numerical results of these experiments are reported in Table 2. Depending on the scenario, the performance has been evaluated by using the same values as the training parameters for all the considered approaches with the exception of the number of epochs for the fine-tuned ResNet that was been reduced to 10 to prevent the network from overfitting. We have performed many experiments with different configurations of ResNet

TABLE 3. Results of the different ResNet configurations for the IDC detection. The best performance is highlighted in bold.

Network	Acc.	F-meas.	Prec.	Sens.	Spec.	BAC
ResNet-18 fine-tuned	86.79	75.38	77.39	73.48	91.85	82.67
ResNet-18 from scratch	85.28	72.94	73.83	72.07	90.30	81.18
ResNet-34 fine-tuned	87.24	77.14	76.08	77.22	90.66	84.44
ResNet-34 from scratch	85.11	72.32	73.65	70.69	90.42	80.55
ResNet-50 fine-tuned	87.52	77.02	78.03	76.08	91.87	83.97
ResNet-50 from scratch	85.00	72.91	73.37	72.47	90.01	81.24

TABLE 4. TP, TN, FP and FN calculated by the different approaches for the IDC detection. The best performance is highlighted in bold.

Scenario	Network	TP	TN	FP	FN
Classification by reconstruction	FusionNet	9964	33610	3672	4193
	UNet	8504	35041	2241	5653
Supervised Classification	SEF	11857	34215	3067	2300
	SEU	9297	34876	2406	4860
	ResNet-34	11074	33800	3482	3083

(i.e. ResNet-18, ResNet-34 and ResNet-50, fine-tuned and from scratch). The results are shown in Table 3. Independently of the configuration, ResNet always outperformed FusionNet, UNet and SEU, following SEF in the ranking. For the sake of simplicity, we report in Tables 2 only the results for the best configuration of ResNet in terms of the F-measure and BAC (i.e. the fine-tuned ResNet-34).

The SEF method significantly outperformed the other DL approaches in terms of the accuracy. Indeed, it achieved an overall increment of 4.86%, 5.52%, 3.7% and 2.33% in accuracy as compared to FusionNet, UNet, SEU and ResNet-34, respectively. Also for the remaining measures, SEF proved to be the best configuration, followed in the ranking by ResNet-34, with the exception of the performance in terms of Specificity, where UNet turns out to be the winning approach.

The numbers of true positive patches (TP), true negative patches (TN), false positive patches (FP) and false negative patches (FN) are reported in Table 4.

Figs. 4 and 5 illustrate examples of the IDC detection result of SEF versus the FusionNet, UNet, SEU and ResNet methods compared to the ground truth. The true positive patches are highlighted in green, while the false positive patches are highlighted in red. All methods showed a reasonable detection performance, but SEF (Figs. 4(d) and 5(d)) revealed much more information compared to the other images, the result being closer to the ground truth. False positive patches produced by FusionNet and ResNet-34 tend to accumulate in specific regions, while those generated by SEF are sparsely distributed. This suggests that SEF allows to adopt such a kind of region based decision rules (e.g. the majority voting), such that a patch is definitely classified as IDC only when this classification label extends over multiple adjacent patches.

TABLE 5. The comparisons with the state of the art for the IDC detection and lymphoma multi-classification. The best performance is highlighted in bold.

	IDC		Lymphoma
	F-meas.	BAC	Acc.
SEF	81.54	87.76	97.67
Method in [13]	76.48	84.68	96.58
Method in [9]	71.80	84.23	-

Finally, in the first column of the Table 5 comparisons between SEF and the other two methods ([13] and [9]) in the literature are reported. Methods [13] and [9] were evaluated using the same dataset D-IDC and are based on AlexNet and a 3-layered CNN, respectively. They were ranked according to the performance of the F-measure and BAC. The SEF approach outperformed method [13] with an increment of 5.06% and 3.08% in terms of the F-measure and BAC, respectively. With respect to method [9], the performance of SEF showed an increment of 9.74% and 3.53% in terms of the F-measure and BAC measure, respectively. Comparing the results of Tables 2 and 5, it is clear that ResNet-34 also outperformed both methods [13] and [9] in terms of the F-measure, while the BAC measure was approximately equivalent in all these methods. Finally, residual CNNs end-to-end trained for classification (i.e., SEF and ResNet) provided the best performances for the IDC detection task. In particular, SEF provided the best performance.

B. LYMPHOMA MULTI-CLASSIFICATION

The D-Lymph dataset has been employed as a benchmark to evaluate the image analysis techniques for the CLL, FL and

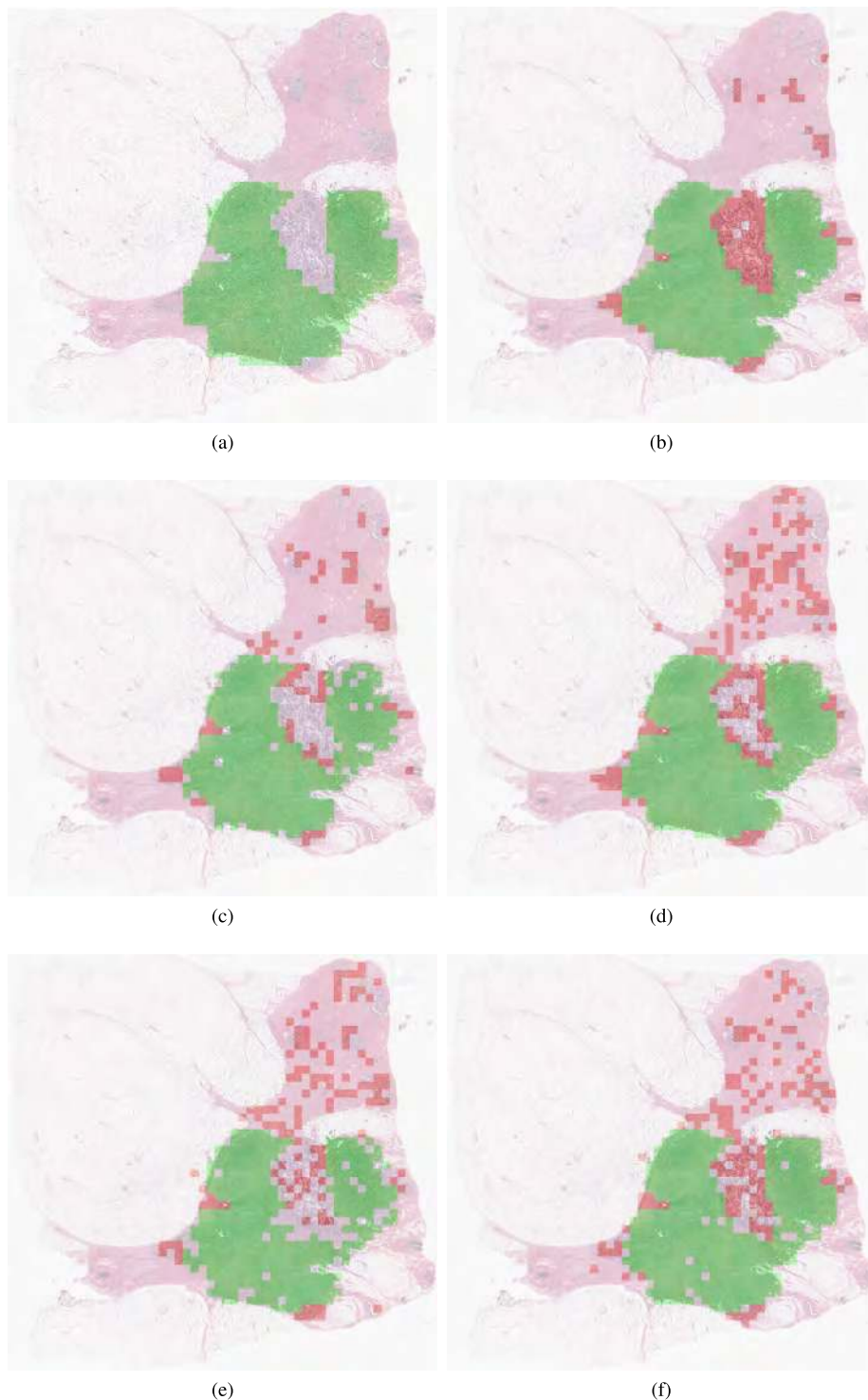


FIGURE 4. Results for the IDC detection (true positive and false positive patches are highlighted in green and in red, respectively): (a) ground truth (b) FusionNet (c) UNet (d) SEF (e) SEU (f) ResNet-34.

MCL sub-types. In total 374 images were generated, containing 113, 139, and 122 images of CLL, FL and MCL, respectively. The size of each image was equal to 1388×1040 pixels. In Fig. 6 a sample for each class is shown. With high resolution images, DL models suffer from high

computational costs and limitations in the number of model layers and channels. In accordance with a general trend, the authors in [13] address this problem by training their DL network on image patches and classifying an image based on patch-level predictions. We decide on a different strategy,

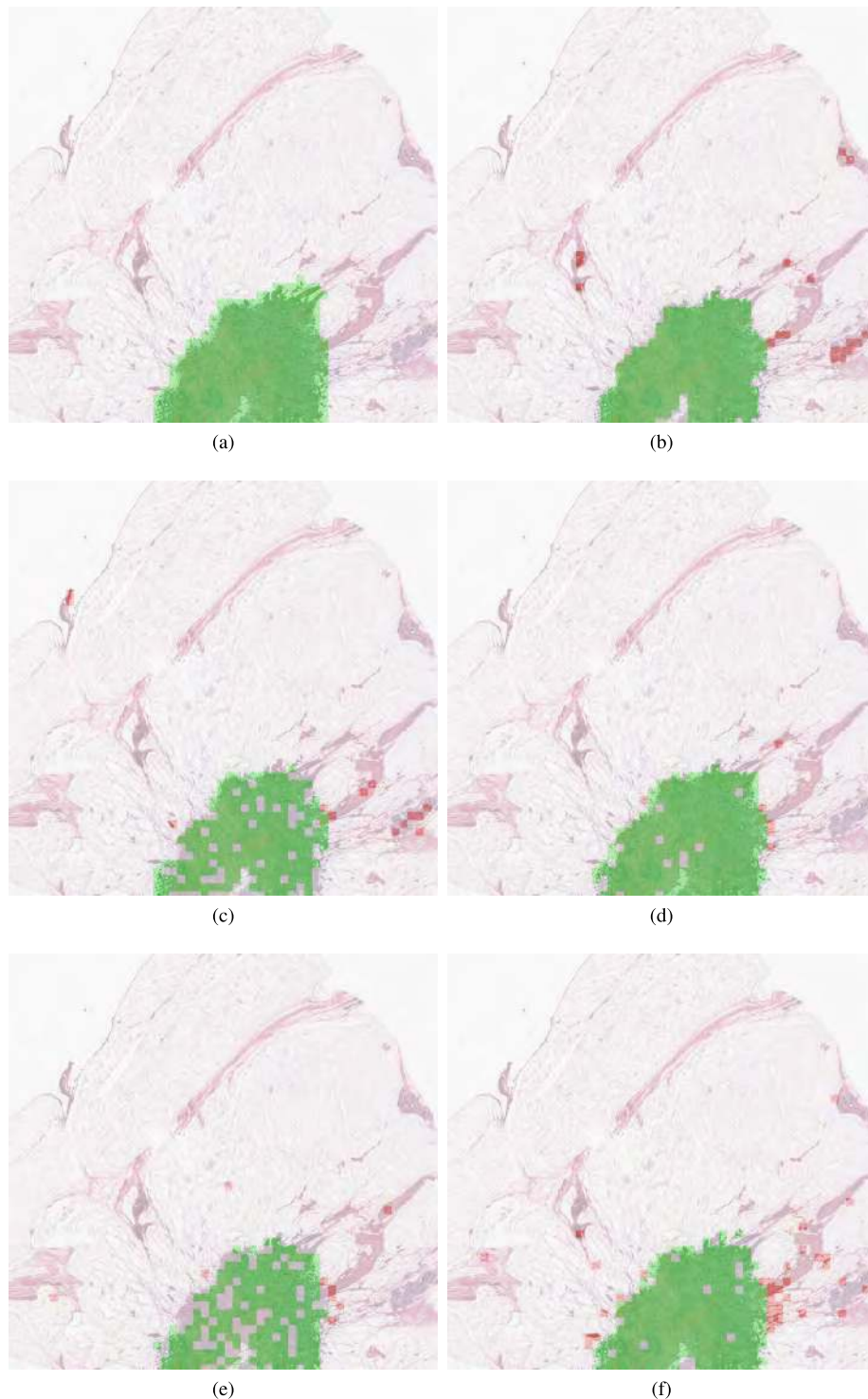


FIGURE 5. Results for the IDC detection (true positive and false positive patches are highlighted in green and in red, respectively): (a) ground truth (b) FusionNet (c) UNet (d) SEF (e) SEU (f) ResNet-34.

that of reducing the input image by a factor about 88%. Doing so, the spatial organization of cellular structures can be globally analyzed by the network, while also keeping the computational cost down. The reduced image had a size equal to 170×128 pixels. We considered the central square section

with a size equal to 128×128 pixels as the input to the network. In this case, the input size of the bridge layer was equal to 8×8 .

An augmentation of the dataset was performed by considering a set of 9 transformations for each training image

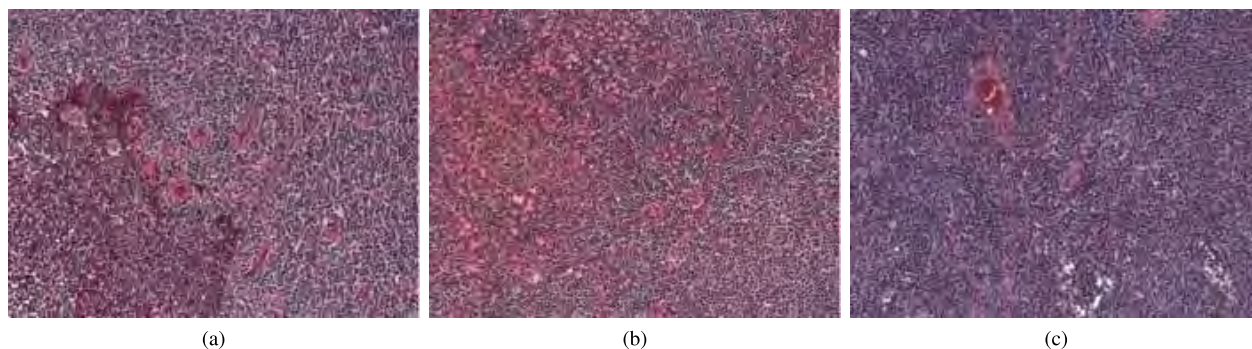


FIGURE 6. Lymphoma sub-types: (a) MCL (b) CLL (c) FL.

TABLE 6. The training parameters for the lymphoma multi-classification.

Scenario	N° Epochs	Mini-batch	Back. alg.	Init. Lear.rate	Lear.rate update
Classification by reconstruction	200	32	SGD	0.001	0.0001 after 150 th epoch
Supervised Classification	150	32	ADAM	0.0001	update by ADAM

TABLE 7. Results of the different approaches for the lymphoma multi-classification. The best performance is highlighted in bold.

Scenario	Network	Acc.	St. Dev.
Classification by reconstruction	FusionNet	77.60	5.4
	UNet	65.10	8.4
Supervised Classification	SEF	97.67	1.3
	SEU	92.80	3.2
	ResNet-34	95.47	2.0

(i.e. horizontal flip, vertical flip, three clock-wise rotations of 90°, and two horizontal and two vertical translations of ±100 pixels). In order to allow a comparison with [13], the same experimental protocol was followed. In particular, in [13] a k-fold cross validation with $k = 5$ was adopted, where each folder contained 299 training images (consisting of about 80% of the whole dataset) and 75 test images. Differently from [13], each folder contained resized central regions of the image together with their corresponding augmentations, instead of patches resulting from a splitting operation. The values of the parameters adopted for the training are given in Table 6. Both scenarios produced 512 feature maps, at the end of the encoding stage. In the “Classification by Reconstruction” scenario, a max pooling layer with a kernel size equal to 4×4 and a stride equal to 2 was applied at the end of the encoding part, producing 2048 feature maps. In the “Supervised Classification” scenario, the max pooling layer was substituted by a fully connected layer, which did not produce any increase in the number of feature maps.

1) EXPERIMENTAL RESULTS AND DISCUSSION

The performances of the different approaches have been quantitatively assessed by considering the Accuracy measure. The numerical results of these experiments are reported in Table 7.

Also in this case, we have performed many experiments with different configurations of ResNet (i.e. ResNet-18, ResNet-34 and ResNet-50, fine-tuned and from scratch and by using two different input sizes i.e. 128×128 and 224×224 pixels). Moreover, by performing Wilcoxon test [27] to validate the statistical significance, we found that the obtained p-values always exceed 0.7. For this reason, we preferred to report in Table 8 the results produced by the fine-tuned ResNet-34, as it provides the lowest standard deviation.

The SEF method achieved an accuracy of 97.67% which is 20.07%, 32.57%, 4.87%, and 2.2% higher when compared with those of FusionNet, U-Net, SEU and ResNet-34, respectively. In this use case also, the SEF and ResNet networks outperformed the other networks. The same values for the training parameters were used for all the considered approaches, with the exception of fine-tuned ResNet-34, which adopted a lower number of epochs (50 epochs) and a different resolution of the input images (224×224 pixels). In order to further strengthen these results, we have also performed Wilcoxon test between SEF and the other methods. The resulting p-values are reported in table 9. With the exception of the comparison between SEF and Resnet-34 (p-value = 0.1288), the obtained p-values are always lower than 0.01. Other observations can be made by looking in Table 7 at the values of the standard deviation of accuracy, computed

TABLE 8. Results of the different ResNet configurations for the lymphoma multi-classification. The best performance is highlighted in bold.

Network	Acc.
ResNet-18 fine-tuned (128 × 128)	93.60
ResNet-18 from scratch (128 × 128)	81.87
ResNet-18 fine-tuned (224 × 224)	95.73
ResNet-18 from scratch (224 × 224)	83.20
ResNet-34 fine-tuned (128 × 128)	93.86
ResNet-34 from scratch (128 × 128)	80.00
ResNet-34 fine-tuned (224 × 224)	95.47
ResNet-34 from scratch (224 × 224)	81.86
ResNet-50 fine-tuned (128 × 128)	93.07
ResNet-50 from scratch (128 × 128)	86.93
ResNet-50 fine-tuned (224 × 224)	94.93
ResNet-50 from scratch (224 × 224)	87.47

TABLE 9. The p-values provided by the Wilcoxon test between SEF and each other methods.

Method	p-value
FusionNet	0.0088
UNet	0.0088
SEU	0.0142
ResNet-34	0.1288

TABLE 10. The confusion matrix of FusionNet.

	MCL	CLL	FL
MCL	16.8	4.4	3.2
CLL	5.2	15.6	1.8
FL	0.8	1.4	25.6

TABLE 11. The confusion matrix of UNet.

	MCL	CLL	FL
MCL	13.4	2.8	8.4
CLL	8	10.8	3.8
FL	2.6	0.6	24.6

TABLE 12. The confusion matrix of SEF.

	MCL	CLL	FL
MCL	23.6	0.8	0.2
CLL	0.4	22	0.2
FL	0.2	0	27.6

by adopting a 5-fold cross validation. The SEF method had a much lower standard deviation of accuracy when compared with those of FusionNet, UNet, SEU and ResNet-34. Thus, the performance of SEF had a lower dependence on the selection of the training set than each of the other approaches. Additionally, the Tables 10, 11, 12, 13 and 14 show the confusion matrices of Fusionnet, UNet, SEF, SEU and ResNet-34, respectively. Considering that the average number of MCL,

TABLE 13. The confusion matrix of SEU.

	MCL	CLL	FL
MCL	20.4	3.2	1
CLL	1.8	20.2	0.6
FL	0.8	0.4	26.6

TABLE 14. The confusion matrix of ResNet-34.

	MCL	CLL	FL
MCL	22.4	1	1.2
CLL	0.6	21.8	0.2
FL	0.4	0	27.4

CLL and FL images, in the test set, is equal to 24.6, 22.2 and 27.8, respectively, by means of an analysis of the confusion matrices it is clear that the number of miss-classified images with SEF was considerably lower than those provided by the other approaches. The performance of SEF is compared with method [13], which adopts AlexNet also for this use case and it is evaluated only in terms of accuracy (see the last column of the Table 5). The SEF method achieved an accuracy of 97.67% which was 1.09%, higher when compared with the accuracy of method [13].

For the sake of completeness, we tested also the same training strategy as [13] for SEF and ResNet-34. Instead of image resizing preprocessing, the images were split into 48 × 48 patches with a stride of 48 avoiding the augmentation of the dataset. During the testing stage, patches were extracted using the same methodology, and a voting scheme per subtype was used where the votes were aggregated to predict the class. In particular, the class with the highest number of votes became the detected class for the entire image. According to this training strategy, ResNet-34 achieved an accuracy equal to 96.84% outperforming method [13]. SEF obtained an accuracy equal to 97.06% and it proved once again to have the best performance.

V. CONCLUSIONS

In this work, we have suggested a method, namely SEF, based on a deep network for learning histological images to avoid hand-crafted pathological features. Using deep learning approaches with specific settings for cancer detection and classification is an effective and reliable strategy compared to conventional approaches. We have shown that the encoder of FusionNet, which has been designed for image segmentation and reconstruction, can be adapted for cancer detection and the classification of histological images.

In detail, our SEF method is based on a Residual CNN (i.e. the encoder of FusionNet) and a softmax classifier to address two use cases: the detection of IDC of the breast cancer and lymphoma multi-classification.

In our experiments, we compared the performances of SEF against different existing deep neural network (FusionNet, UNet and ResNet) and the encoding part of UNet under the same conditions and on the same datasets.

We have also proposed several strategies for training of the proposed network, based on the extraction of patches or on resized images, allowing us to deal with the high-resolution of histological images. The detailed experimental analysis and performance comparisons show a significant improvement of the SEF method in relation to all the considered DL approaches and other existing methods for both use cases. The results show that for the considered uses cases, Autoencoders (FusionNet and UNet) extract features that are unsuitable for the classification, as they are learned for the image reconstruction. This is the underlying reason why CNNs trained end-to-end for classification have provided a higher performance. In particular, the residual one (SEF and RESNet) are better at consider for small cellular structures depicted in the histological images, as they attenuate the drawback of vanishing gradients. However, this problem remains, so increasing the deep of the network (from 34 to 50 layers in RESNet) does not translate into an increasing of the classification performance. In our future work we aim to explore the application of SEF to other use cases for histological image analysis and also with different training strategies.

REFERENCES

- [1] (2014). *ICPR MITOS-ATYPIA*. [Online]. Available: <http://mitosatypia-14.grand-challenge.org/>
- [2] *Lymphoma and IDC Datasets*. Accessed: 2016. [Online]. Available: <http://www.andrewjanowczyk.com/deep-learning/>
- [3] G. Aresta et al. (2018). "BACH: Grand challenge on breast cancer histology images." [Online]. Available: <https://arxiv.org/abs/1808.04277>
- [4] D. Bardou, K. Zhang, and S. M. Ahmad, "Classification of breast cancer based on histology images using convolutional neural networks," *IEEE Access*, vol. 6, pp. 24680–24693, 2018.
- [5] N. Bayramoglu, J. Kannala, and J. Heikkilä, "Deep learning for magnification independent breast cancer histopathology image classification," in *Proc. 23rd Int. Conf. Pattern Recognit. (ICPR)*, Dec. 2016, pp. 2440–2445.
- [6] B. E. Bejnordi et al., "Stain specific standardization of whole-slide histopathological images," *IEEE Trans. Med. Imag.*, vol. 35, no. 2, pp. 404–415, Feb. 2016.
- [7] N. Brancati, M. Frucci, and D. Riccio, "Multi-classification of breast cancer histology images by using a fine-tuning strategy," in *Image Analysis and Recognition*, A. Campilho, F. Karray, and B. ter Haar Romeny, Eds. Cham, Switzerland: Springer, 2018, pp. 771–778.
- [8] H. Chen et al., "Mitosis detection in breast cancer histology images via deep cascaded networks," in *Proc. AAAI*, 2016, pp. 1160–1166.
- [9] A. Cruz-Roa et al., "Automatic detection of invasive ductal carcinoma in whole slide images with convolutional neural networks," *Proc. SPIE*, vol. 9041, Mar. 2014, Art. no. 904103.
- [10] A. A. Cruz-Roa, J. E. A. Ovalle, A. Madabhushi, and F. A. G. Osorio, "A deep learning architecture for image representation, visual interpretability and automated basal-cell carcinoma cancer detection," in *Proc. Int. Conf. Med. Image Comput. Comput.-Assist. Intervent. Berlin, Germany: Springer*, 2013, pp. 403–410.
- [11] K. He, X. Zhang, S. Ren, and J. Sun, "Deep residual learning for image recognition," in *Proc. IEEE Conf. Comput. Vis. Pattern Recognit.*, Jun. 2016, pp. 770–778.
- [12] L. Hou et al., "Sparse autoencoder for unsupervised nucleus detection and representation in histopathology images," *Pattern Recognit.*, vol. 86, pp. 188–200, Feb. 2019.
- [13] A. Janowczyk and A. Madabhushi, "Deep learning for digital pathology image analysis: A comprehensive tutorial with selected use cases," *J. Pathol. Inform.*, vol. 7, p. 29, Jul. 2016.
- [14] D. P. Kingma and J. Ba. (2014). "Adam: A method for stochastic optimization." [Online]. Available: <https://arxiv.org/abs/1412.6980>
- [15] A. Krizhevsky, I. Sutskever, and G. E. Hinton, "ImageNet classification with deep convolutional neural networks," in *Proc. Adv. Neural Inf. Process. Syst.*, 2012, pp. 1097–1105.
- [16] Y. LeCun, L. Bottou, Y. Bengio, and P. Haffner, "Gradient-based learning applied to document recognition," *Proc. IEEE*, vol. 86, no. 11, pp. 2278–2324, Nov. 1998.
- [17] Y. Liu et al. (2017). "Detecting cancer metastases on gigapixel pathology images." [Online]. Available: <https://arxiv.org/abs/1703.02442>
- [18] R. Nateghi, H. Danyali, and M. S. Helfroush, "Maximized inter-class weighted mean for fast and accurate mitosis cells detection in breast cancer histopathology images," *J. Med. Syst.*, vol. 41, no. 9, p. 146, 2017.
- [19] A. Ng, "Sparse autoencoder," *CS294A Lect. Notes*, vol. 72, 2011.
- [20] T. M. Quan, D. G. Hilderbrand, and W.-K. Jeong. (2016). "FusionNet: A deep fully residual convolutional neural network for image segmentation in connectomics." [Online]. Available: <https://arxiv.org/abs/1612.05360>
- [21] O. Ronneberger, P. Fischer, and T. Brox, "U-NET: Convolutional networks for biomedical image segmentation," in *Proc. Int. Conf. Med. Image Comput. Comput.-Assist. Intervent. Springer*, 2015, pp. 234–241.
- [22] F. A. Spanhol, L. S. Oliveira, L. Heutte, and C. Petitjean, "A dataset for breast cancer histopathological image classification," *IEEE Trans. Biomed. Eng.*, vol. 63, no. 7, pp. 1455–1462, Jul. 2016.
- [23] F. A. Spanhol, L. S. Oliveira, C. Petitjean, and L. Heutte, "Breast cancer histopathological image classification using convolutional neural networks," in *Proc. Int. Joint Conf. Neural Netw. (IJCNN)*, Jul. 2016, pp. 2560–2567.
- [24] M. Veta et al., "Assessment of algorithms for mitosis detection in breast cancer histopathology images," *Med. Image Anal.*, vol. 20, no. 1, pp. 237–248, 2015.
- [25] T. H. Vu, H. S. Mousavi, V. Monga, G. Rao, and U. K. A. Rao, "Histopathological image classification using discriminative feature-oriented dictionary learning," *IEEE Trans. Med. Imag.*, vol. 35, no. 3, pp. 738–751, Mar. 2016.
- [26] D. Wang, A. Khosla, R. Gargeya, H. Irshad, and A. H. Beck. (2016). "Deep learning for identifying metastatic breast cancer." [Online]. Available: <https://arxiv.org/abs/1606.05718>
- [27] F. Wilcoxon, "Individual comparisons by ranking methods," *Biometrics Bull.*, vol. 1, no. 6, pp. 80–83, 1945.
- [28] J. Xu et al., "Stacked sparse autoencoder (SSAE) for nuclei detection on breast cancer histopathology images," *IEEE Trans. Med. Imag.*, vol. 35, no. 1, pp. 119–130, Jan. 2016.
- [29] K.-H. Yu et al., "Predicting non-small cell lung cancer prognosis by fully automated microscopic pathology image features," *Nature Commun.*, vol. 7, Aug. 2016, Art. no. 12474.
- [30] Y. Zhang, B. Zhang, F. Coenen, J. Xiao, and W. Lu, "One-class kernel subspace ensemble for medical image classification," *EURASIP J. Adv. Signal Process.*, vol. 2014, no. 1, p. 17, 2014.



NADIA BRANCATI received the Laurea degree (*cum laude*) in computer science from the University of Naples Parthenope, in 2008. She is currently a Researcher with the National Research Council of Italy. Her research interests include mainly image processing, computer vision, and human-computer interaction, in particular segmentation, image analysis, color image processing, classification, and medical imaging. She is a member of the Italian Association of Computer Vision, Pattern Recognition, and Machine Learning (CVPL).



GIUSEPPE DE PIETRO is currently the Director of the Institute for High Performance Computing and Networking-CNR and an Adjunct Professor with the College of Science and Technology, Temple University, Philadelphia. He is actively involved in many European and National projects, with industrial co-operations too. He has authored more than 180 scientific papers published in international journals and conferences. His current research interests include cognitive computing, clinical decision support systems, and software architectures for e-health. He is an IEEE and KES International Member. He is involved in many program committees and journal editorial boards.



MARIA FRUCCI received the Ph.D. degree (*cum laude*) in physics from the University of Naples Federico II, Italy, in 1983. She is currently a Senior Researcher with the National Research Council of Italy. She has published more than 100 papers on different topics, such as natural language, perception, representation, image analysis, segmentation, biometrics, color image processing, and medical imaging. Her research interests include image processing, computer vision, and pattern recognition.

She is a member of the Italian Association of Computer Vision, Pattern Recognition, and Machine Learning (CVPL).



DANIEL RICCIO received the Laurea degree (*cum laude*) and the Ph.D. degree in computer sciences from the University of Salerno, Salerno, Italy, in 2002 and 2006, respectively. He is currently an Associate Professor with the University of Naples Federico II. He is also an Associate Researcher with the National Research Council of Italy. His research interests include biometrics, medical imaging, image processing and indexing, and image and video analytics. He is an IEEE

Member and a member of the Italian Association of Computer Vision, Pattern Recognition, and Machine Learning (CVPL).

• • •